

# Global monitoring of air pollution over land from the Earth Observing System-Terra Moderate Resolution Imaging Spectroradiometer (MODIS)

D. A. Chu,<sup>1,2</sup> Y. J. Kaufman,<sup>2</sup> G. Zibordi,<sup>3</sup> J. D. Chern,<sup>4</sup> Jietai Mao,<sup>5</sup> Chengcai Li,<sup>5</sup> and B. N. Holben<sup>6</sup>

Received 16 November 2002; revised 7 June 2003; accepted 24 June 2003; published 5 November 2003.

[1] Moderate Resolution Imaging Spectroradiometer (MODIS) measurements (7 channels: 0.47–2.1  $\mu\text{m}$ , 250–500 m resolutions) provide us with new insights into the characteristics of global aerosols. MODIS retrieves not only aerosol loading but also the fraction of fine mode particle. In this paper we demonstrate MODIS capability for use in monitoring global, regional, and local air pollution. Three case studies in northern Italy, Los Angeles, and Beijing showed the conclusive results of applying MODIS-derived aerosol optical depths ( $\tau_a$ ) to regional and local air pollution in terms of accuracy ( $\Delta\tau_a = \pm 0.05 \pm 0.2\tau_a$ ) and spatial sensitivity of the retrievals. Under stagnant condition, accumulated aerosol abundance can reach  $\tau_a > 1$  (at 0.55  $\mu\text{m}$ ) before being removed by wind or precipitation. The correlation found between Aerosol Robotic Network (AERONET) daily averaged  $\tau_a$  and 24-hour  $\text{PM}_{10}$  (particulate matter with diameter  $< 10 \mu\text{m}$ ) concentration ( $\mu\text{g}/\text{m}^3$ ) in northern Italy is encouraging with correlation coefficient  $\sim 0.82$ . The derivation of PM concentration from satellite measurements may be possible once we know the detailed aerosol vertical distribution. To compare aerosol loading in different regions of the globe, we choose the two most populated regions (eastern China and India) and the two most industrialized regions (the eastern United States/Canada and western Europe). The time series of MODIS monthly mean  $\tau_a$  from July 2000 to May 2001 depicts a strong seasonal variation with maxima in the spring/summer and minima in the winter. The clear separation between (1) the eastern United States/Canada and western Europe and (2) eastern China and India shows that the  $\tau_a$  values in (2) are 50% to 2–3 times higher compared to those in (1). The enhancements of aerosol loading were due to smoke as originated from Montana/Idaho forest fires transported to the eastern United States in late August 2000 and dust outbreaks from Taklimakan and Gobi Deserts to eastern China as well as smoke from Southeast Asia to southern China in February–April 2001. *INDEX TERMS*: 0305 Atmospheric Composition and Structure: Aerosols and particles (0345, 4801); 0345 Atmospheric Composition and Structure: Pollution—urban and regional (0305); 0365 Atmospheric Composition and Structure: Troposphere—composition and chemistry; 1610 Global Change: Atmosphere (0315, 0325); 1640 Global Change: Remote sensing; *KEYWORDS*: satellite remote sensing, air pollution, aerosol properties

**Citation:** Chu, D. A., Y. J. Kaufman, G. Zibordi, J. D. Chern, J. Mao, C. Li, and B. N. Holben, Global monitoring of air pollution over land from the Earth Observing System-Terra Moderate Resolution Imaging Spectroradiometer (MODIS), *J. Geophys. Res.*, 108(D21), 4661, doi:10.1029/2002JD003179, 2003.

<sup>1</sup>Science Systems and Applications, Inc., Lanham, Maryland, USA.

<sup>2</sup>Laboratory for Atmospheres, NASA Goddard Space Flight Center, Greenbelt, Maryland, USA.

<sup>3</sup>Institute for Environment and Sustainability, Joint Research Centre, Ispra, Italy.

<sup>4</sup>Goddard Earth Sciences and Technology Center, Laboratory for Atmospheres, NASA Goddard Space Flight Center, Greenbelt, Maryland, USA.

<sup>5</sup>Department of Atmospheric Science, School of Physics, Peking University, Beijing, China.

<sup>6</sup>Laboratory for Terrestrial Physics, NASA Goddard Space Flight Center, Greenbelt, Maryland, USA.

## 1. Introduction

[2] Satellite remote sensing has established long records of aerosol measurements since the late 1970s. However, most of the aerosol properties were derived over the ocean (e.g., Advanced Very High-Resolution Radiometer (AVHRR)) until the discovery of Total Ozone Mapping Spectrometer (TOMS) new capability in detecting elevated absorbing aerosols over both land and ocean using ultraviolet spectrum (0.34 and 0.38  $\mu\text{m}$ ) [Hsu *et al.*, 1996; Herman *et al.*, 1997]. In recent years, a major advancement emerging in satellite remote sensing is the systematic retrieval of aerosol properties over land by MODIS on board Earth Observing System (EOS) Terra and Aqua satellites [King *et*

al., 1999]. The unique set of seven MODIS well-calibrated channels (0.47, 0.55, 0.67, 0.87, 1.24, 1.64, 2.1  $\mu\text{m}$ ) provides the spectral information of aerosol optical properties and underlying surfaces from visible to shortwave infrared wavelength. The MODIS-derived aerosol properties ( $\tau_a$  and the fraction of fine mode particle) over land [Kaufman et al., 1997a; Chu et al., 1998, 2002] in tandem with those ( $\tau_a$ , the fraction of fine mode particle, and effective radius) over ocean [Tanré et al., 1997, 1999; Remer et al., 2002] enable us to comprehensively study the global aerosols.

[3] Measurements of high spatial and temporal coverage are important to analyze aerosols because of their large variability (close to sources and sinks) and short lifetimes (a few hours to a few weeks). In contrast to surface instruments that acquire continuous measurements at fixed locations, polar-orbiting Sun-synchronous satellite sensors provide a global coverage at nearly constant local solar times (once or twice a day in tropics to midlatitude and multiple overpasses in polar regions). The advantage of satellite measurements is relating local in situ/remote sensing measurements in distance. For example, TOMS aerosol loading measurements (1979–present) were used to study the transport of dust and smoke aerosols [Hsu et al., 1996; Herman et al., 1997]. The uncertainties of TOMS aerosol loading, however, are attributed to large footprint ( $\sim 50 \text{ km} \times 50 \text{ km}$ ) and strong altitude dependence [Hsu et al., 1996; Torres et al., 1998]. Multiangle Imaging Spectroradiometer (MISR) [Diner et al., 1998] also on board EOS-Terra satellite is capable of deriving aerosol properties over both land and ocean but it requires 6–9 days to complete a global coverage. In contrast, MODIS measurements with a swath width of 2330 km provide a near global coverage (95%) everyday. Using both MODIS sensors from EOS-Terra (10:30 a.m. equator-crossing time) and EOS-Aqua (1:30 p.m. equator-crossing time) enables us to study aerosol diurnal variation, if any, on a global scale.

[4] Despite that oceans cover 70% of Earth's surface, most of the tropospheric aerosols are originated from land with a large variety of chemical compositions (soot, organic, and inorganic compounds, etc.) and particle sizes (submicron to microns). In turn, their radiative effects are also varying. The aerosol radiative effects have been extensively studied using numerical/empirical models [Hansen and Lacis, 1990; Penner et al., 1994; Tegen et al., 1996; Charlson et al., 1992] and satellite/ground-based measurements [Christopher et al., 1996; Hsu et al., 2000]. The scarcity of satellite aerosol retrievals over land may have been one of the contributors to the large uncertainties estimated for aerosol radiative effects [Intergovernmental Panel on Climate Change, 2001]. Tropospheric aerosols (also known as particulate matter (PM)) can cause severe impacts on ecosystems, for example, through acid deposition in reducing agricultural productivity [Chameides et al., 1999], or endangering aquatic lives [Adriano and Johnson, 1989]. The detrimental effect on human health when exposed to high concentrations of airborne PM is also evident [Beeson et al., 1998]. Establishing the link between aerosol optical depth derived from satellite and PM concentration measured at surface would be an important step for public health related studies.

[5] The purpose of this paper is to demonstrate MODIS capability in retrieving aerosol optical depths over land and

applies the retrievals to global, regional, and local air pollution. Three case studies are targeted with different spatial scales: (1) northern Italy ( $\sim 600 \times 400 \text{ km}^2$ ), (2) city of Los Angeles ( $\sim 100 \times 50 \text{ km}^2$ ) and (3) urban area of Beijing ( $\sim 30 \times 30 \text{ km}^2$ ) to show the accuracy and spatial sensitivity of aerosol retrievals. The NASA Data Assimilation Office (DAO) Goddard Earth Observing System-3 (GEOS-3)  $1^\circ \times 1^\circ$  assimilated data are used to analyze wind and temperature fields associated with the air pollution events. The methodology of the MODIS aerosol retrieval over land is discussed, along with important changes made in different data processing cycles. MODIS aerosol retrievals are compared with AEROENT measurements as the baseline validation. Local Sun photometer measurements are also used as alternative validation sources in regions where AERONET data are not available. At last, MODIS monthly average  $\tau_a$  are derived to illustrate the regional and temporal variabilities of air pollution in the eastern United States/Canada, western Europe, eastern China, and India between July 2000 and May 2001.

## 2. Retrieval Methodology

[6] Aerosol radiative effect includes scattering and absorption of direct sunlight and sunlight reflected by underlying surface. The radiative transfer equation that governs the calculation of apparent reflectance at top of atmosphere (TOA) can be expressed as

$$\rho^*(\theta, \theta_o, \phi) = \rho_a(\theta, \theta_o, \phi) + \frac{F_d(\theta_o) T(\theta) \rho(\theta, \theta_o, \phi)}{1 - sp'}$$

where  $\rho^*$  is apparent reflectance ( $\pi L/F_o \mu_o$ ,  $L$ : radiance measured at TOA;  $F_o$ : extraterrestrial solar flux;  $\mu_o$ : cosine of solar zenith angle);  $\rho$  is the path radiance (in unit of reflectance) due to aerosol and molecular scattering;  $F_d$  is normalized downward total flux for zero surface reflectance (equivalent to total downward transmission);  $T$  is upward total transmission into the direction of satellite field of view;  $s$  is atmospheric backscattering ratio;  $\rho'$  is surface reflectance averaged on the view and illumination angles ( $\theta_v$ : view direction;  $\theta_o$ : solar zenith angle;  $\varphi$ : relative azimuth angle of scattered radiation from incident solar beam). Owing to the competing processes of surface reflection and aerosol backscattering in radiative transfer, radiance measured with less surface interference results in smaller uncertainty in the retrieved aerosol properties. The dark target approach presented here follows Kaufman et al. [1997a]. The MODIS retrieval of  $\tau_a$  over land employs primarily three spectral channels centered at 0.47, 0.66, and 2.1  $\mu\text{m}$  wavelengths at 500 m resolution. Aerosol optical depths are derived at 0.47 and 0.66  $\mu\text{m}$ . The use of reflectance measured at 2.1  $\mu\text{m}$  is to infer surface reflectance in the visible since fine-mode particles (urban/industrial and biomass-burning aerosols) are transparent at 2.1  $\mu\text{m}$  allowing direct observation of surface. Figure 1 displays two images with and without smoke appearance. The only difference is due to spectral wavelength ( $<1 \mu\text{m}$  in Figure 1a and  $>1 \mu\text{m}$  in Figure 1b). For dust particles, stronger interaction with sunlight may result in larger uncertainty when using 2.1  $\mu\text{m}$  channel; a full assessment of retrieval errors and possible correction to optical depth caused by

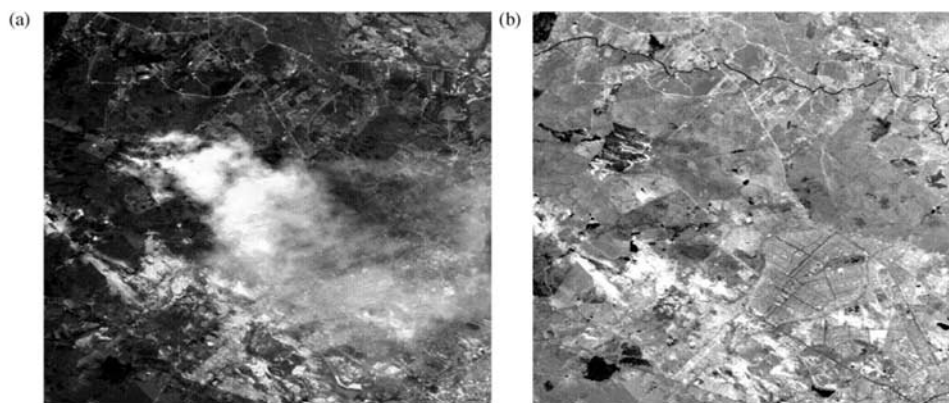


**Figure 1.** (a) True color RGB (R, 0.66  $\mu\text{m}$ ; G, 0.55  $\mu\text{m}$ ; B, 0.47  $\mu\text{m}$ ) image with smoke and (b) false color RGB (R, 2.1  $\mu\text{m}$ ; G, 1.64  $\mu\text{m}$ ; B, 1.24  $\mu\text{m}$ ) image without smoke. These images were acquired from Advanced Visible and Infrared Image Spectrometer (AVIRIS) on board ER-2 during the Smoke, Clouds, And Radiation-Brazil (SCAR-B) field experiment in 1995.

opacity at 2.1  $\mu\text{m}$  are currently underway using the measurements acquired in Aerosol Characterization Experiment-Asia (ACE-Asia) as a test bed. The scope of this paper is focused on fine-mode dominant aerosols.

[7] Owing to large surface variability, a  $10 \times 10 \text{ km}^2$  box (at nadir) is used to better select dark pixels. Among the 400 pixels (at 500 m resolution), cloud-free pixels are first selected using MODIS cloud mask [Ackerman *et al.*, 1998], followed by the screening of water-body pixels using the normalized difference vegetation index (NDVI)  $> 0.1$ , and snow/ice pixels using Near Real-Time Ice and Snow Extent (NISE) from National Snow and Ice Data Center (NSIDC) and National Centers for Environmental Prediction (NCEP) data. MODIS cloud mask utilizes  $\sim 20$  tests (including cirrus clouds) to discriminate clear from cloudy pixels. Under conditions that obstruction in the MODIS field-of-view cannot be distinguished due to clouds or heavy aerosol ( $\tau_a > 3$ ), the resulting cloud mask is reported to be cloudy. Therefore MODIS cloud mask is often described as a “conservative” clear-sky mask. For the remaining clear (cloud-free, water-free, and snow-free) pixels, we use an empirical relationship to estimate surface reflectance ( $\rho_s$ ) at 0.47 and 0.66  $\mu\text{m}$  based upon the reflectance measured at 2.1  $\mu\text{m}$  (i.e.,  $\rho_{0.47\mu\text{m}}/\rho_{2.1\mu\text{m}}^* = 0.25$  and  $\rho_{0.66\mu\text{m}}'/\rho_{2.1\mu\text{m}}^* = 0.5$ ) in an incremental step (i.e.,  $0.01 \leq \rho_{2.1\mu\text{m}}^* \leq 0.05$ ,  $0.01 \leq \rho_{2.1\mu\text{m}}^* \leq 0.1$ , or  $0.01 \leq \rho_{2.1\mu\text{m}}^* < 0.15$ ) This empirical relationship was first developed over vegetated surface (e.g., forest, grassland, etc) using Landsat thematic mapper (TM) and Airborne Visible-Infrared Imaging Spectrometer (AVIRIS) images [Kaufman *et al.*, 1997b] in the United States, then shown also to be valid for semiarid surface [Karnieli *et al.*, 2001]. Recent model simulations support this relationship over uniform dense vegetation [Kaufman *et al.*, 2002], whereas over mixed dark surfaces the discrepancy of surface reflectance estimate is somewhat alleviated by shadows because of uneven canopies and terrain in large-scale measurements. The error of surface reflectance estimate using the empirical relationship increases with increasing 2.1  $\mu\text{m}$  threshold, for example, 16% for  $\rho_s^{2.1\mu\text{m}} < 0.10$  and doubled for  $0.10 < \rho_s^{2.1\mu\text{m}} < 0.15$  at 0.66  $\mu\text{m}$  wavelength [Kaufman *et al.*, 1997b]. At 0.47  $\mu\text{m}$ , somewhat smaller errors are obtained except over red soils

[Gatebe *et al.*, 2001] and burn scars that the overestimation of surface reflectance is often found.

[8] The selected pixels in a  $10 \times 10 \text{ km}^2$  box may still be partially contaminated by subpixel clouds, snow/ice, or soil types that do not fit the empirical relationship. Thus only the lowest 10–40 (in versions 2 and 3) or 20–50 (in version 4) percentile of radiances is used. The selection of 2.1  $\mu\text{m}$  thresholds (e.g.,  $0.01 \leq \rho_{2.1\mu\text{m}}^* \leq 0.05$ ,  $0.01 \leq \rho_{2.1\mu\text{m}}^* \leq 0.1$ ,  $0.01 \leq \rho_{2.1\mu\text{m}}^* < 0.15$ , etc.) is controlled by  $N$  ( $=12$ , 10% of the lowest 10–40 (or 20–50 percentile) of clear pixels out of 400 pixels). In other words, if there are enough pixels ( $N \geq 12$ ) for the lowest threshold (i.e.,  $0.01 \leq \rho_{2.1\mu\text{m}}^* \leq 0.05$ ), the process will stop. Otherwise it will move up to the next threshold, and so on and so forth. It was designed as part of the quality assessment of aerosol retrievals. No retrieval is done if the criterion ( $N = 12$ ) is not met.

[9] The averaged reflectances of  $10 \times 10 \text{ km}^2$  grid boxes are used to derive  $\tau_a$  at 0.47 and 0.66  $\mu\text{m}$  by matching to the values from pre-calculated lookup tables under the same Sun-satellite geometrical conditions. The lookup tables are generated by Dave code [Dave and Gazdag,

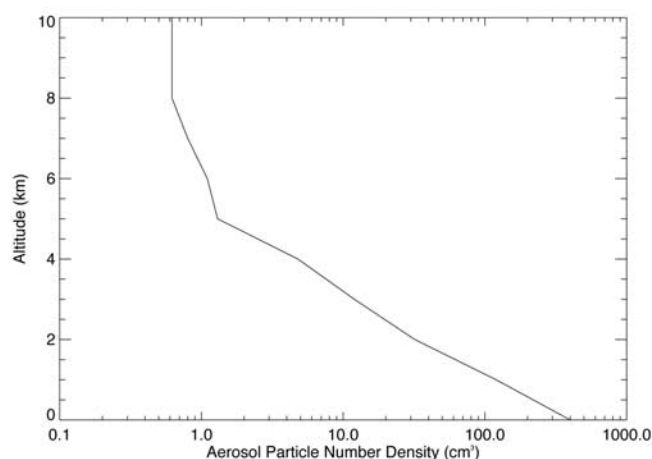


**Figure 2.** “Average” aerosol number density profile used in generating MODIS lookup tables.

**Table 1.** Size Distribution and Single Scattering Albedo Used in the MODIS Look-Up Table for Aerosol Retrieval<sup>a</sup>

	$r_g, \mu\text{m}$	$r_v, \mu\text{m}$	$\sigma$	$\omega_o, 0.47 \mu\text{m}$	$\omega_o, 0.66 \mu\text{m}$
<i>Continental Aerosol Model</i>					
Water soluble	0.005	0.176	1.09	0.96	0.96
	0.5	17.6	1.09	0.69	0.69
Soot	0.0118	0.05	0.69	0.16	0.16
<i>Urban/Industrial Aerosol Model</i>					
Accumulation 1	0.036	0.106	0.60	0.96	0.96
Accumulation 2	0.114	0.21	0.45	0.97	0.97
Salt	0.99	1.30	0.30	0.92	0.92
Coarse	0.67	9.50	0.94	0.88	0.88
<i>Biomass Burning Aerosol Model – Moderate Absorption</i>					
Accumulation	0.061	0.13	0.50	0.90	0.90
Coarse	$1.0-1.3\tau_a$	$6-11\tau_a + 61\tau_a$	$0.69 + 0.81\tau_a$	0.84	0.84
<i>Biomass Burning Aerosol Model – Strong Absorption</i>					
Accumulation	0.061	0.13	0.50	0.86	0.85
Coarse	$1.0-1.3\tau_a$	$6-11\tau_a + 61\tau_a$	$0.69 + 0.81\tau_a$	0.84	0.84
<i>Desert Dust</i>					
Mode 1	0.001	0.006	0.76	0.015	0.015
Mode 2	0.022	1.23	1.16	0.95	0.95
Mode 3	6.24	21.5	0.64	0.62	0.62

<sup>a</sup>Note that:  $r_g$ , geometric radius;  $r_v$ , radius in volume;  $\sigma$ , the standard deviation of the natural logarithm of the radius; and  $\omega_o$ , single scattering albedo.

1970] assuming spherical particle shape, “average” aerosol profile [Braslau and Dave, 1973], and lognormal size distribution. Figure 2 shows the “average” aerosol number density profile used in lookup table generation. The radiative transfer calculations require the input of altitude distribution of aerosol in order to scale the desired aerosol optical depths (e.g.,  $\tau_a = 0, 0.25, 0.5, 1.0, 2.0, 3.0, 5.0$  used in lookup tables) for the calculation of reflectance at TOA. Table 1 displays the size distribution and single scattering albedo of continental, sulfate, smoke, and dust models used. Sulfate and smoke models are dominated by fine mode

particles while dust model is primarily composed of coarse mode particles.

[10] The determination of aerosol type requires two steps: (1) separating urban/industrial and biomass-burning aerosols, and (2) distinguishing between dust and nondust aerosols. Urban/industrial and biomass-burning aerosols (both dominated by fine-mode particles) that cannot be distinguished by path radiance ratio are separated by geographic location and the season of emission. The spectral aerosol path radiance can separate fine mode from coarse mode particles, similar to Ångström exponent, except with an advantage that path radiance is not affected by the assumption of aerosol model. Figure 3 shows the ratio of

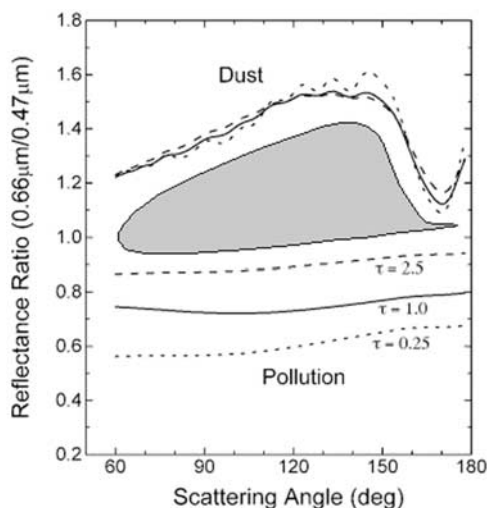


**Figure 3.** The path radiance ratios calculated for dust and pollution aerosols based upon single scattering approximation,  $(\tau_a P \omega_o)_{0.66\mu\text{m}} / (\tau_a P \omega_o)_{0.47\mu\text{m}}$ , ( $P$ , phase function;  $\omega_o$ , single scattering albedo).

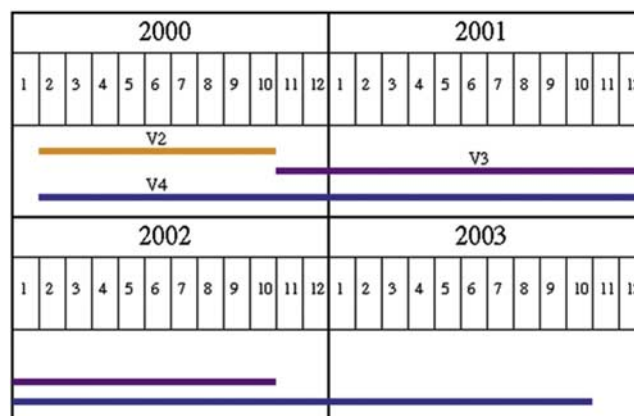


**Figure 4.** Three data processing cycles implemented since MODIS began to acquire measurements on 24 February 2000. “Consistent year” production without algorithm change covers November 2000 through October 2001.

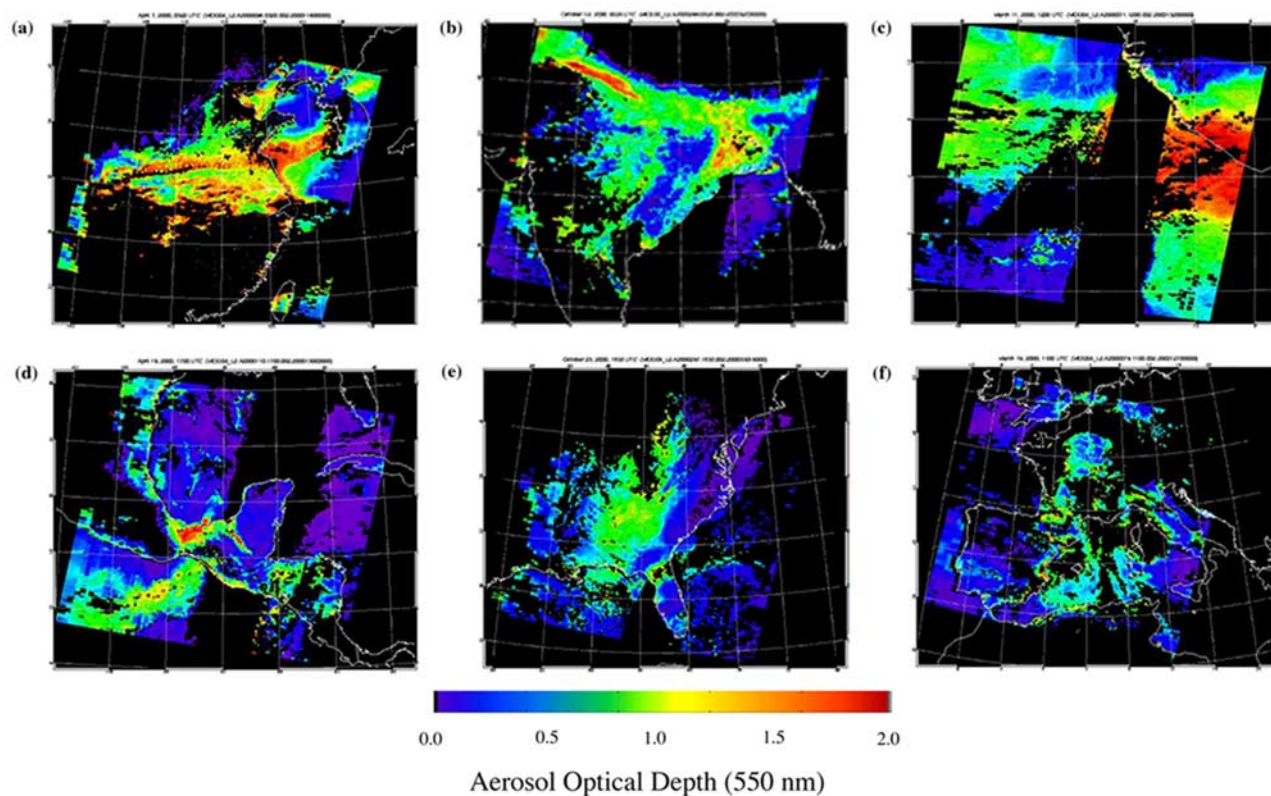


**Figure 5.** Images of MODIS L2  $\tau_a$  (at  $0.55 \mu\text{m}$ ) of six aerosol events: (a) Asian dust outbreak and air pollution (7 April 2000), (b) Indian air pollution (12 October 2000), (c) African smoke and dust (11 March 2000), (d) central American smoke (19 April 2000), (e) eastern United States air pollution (23 October 2000), and (f) western Europe air pollution (19 March 2000).

single-scattering path radiance  $(\tau_a P \omega_o)_{0.66\mu\text{m}} / (\tau_a P \omega_o)_{0.47\mu\text{m}}$  ( $P$ : phase function;  $\omega_o$ : single scattering albedo) derived from dust and pollution models (or moderate absorption smoke model  $\omega_o \sim 0.9$ ) as a function of scattering angle. Shaded in gray is the area needed to account for the mixture of dust and nondust aerosols for  $\tau_a = 2.5$ . Wider separations are found for smaller  $\tau_a$  and scattering angles  $\leq 150^\circ$ . The Fine mode fraction ( $\eta$ ) is derived by linear interpolation based upon the path radiance ratio obtained from a  $10 \times 10 \text{ km}^2$  grid box.

[11] The empirical relationship of surface reflectance and aerosol models used in the retrieval achieved satisfactory success globally over vegetated and semi-vegetated regions with retrieval errors within  $\Delta\tau_a = \pm 0.05 \pm 0.20$  ( $\tau_a$ , e.g., 100% for  $\tau_a = 0.05$  and 15–25% for  $\tau_a = 1$ ) except in the coastal zones where the overestimation of retrieved  $\tau_a$  is primarily attributed to subpixel water contamination [Chu *et al.*, 2002]. MODIS aerosol retrievals are not sensitive to vertical distribution because Rayleigh scattering is much less important in the visible than ultraviolet spectrum. This can be seen from radiative transfer simulations that different aerosol profiles result in the same aerosol optical depth retrieval in the visible wavelength, whereas strong altitude dependence of aerosol layers is found in the ultraviolet regime (e.g., TOMS). As a result, the multiyear MODIS or MODIS Airborne Simulator (MAS) aerosol data show no altitude dependence, even in extreme cases with smoke layers extending from surface up to 5 km altitude observed by airborne clouds physics lidar (CPL) in SCAR-B or

Southern African Regional Science Initiative (SAFARI) 2000 experiments.

### 3. Aerosol Products and Data Processing Cycles

[12] MODIS-derived aerosol properties are reported in level 2 (L2) granule-based (granule: 5-minute segment of one orbit of data) and level 3 (L3) global daily, 8-day, and monthly gridded products. The L2 product contains retrieved aerosol properties (e.g.,  $\tau_a$ ,  $\eta$ , etc.) at  $10 \times 10 \text{ km}^2$ , and L3 contains the statistics (mean, standard deviation, maximum, minimum, etc.) at  $1^\circ \times 1^\circ$  spatial resolution. The details of file specification of MODIS L2 and L3 aerosol products can be found at the Web site <http://modis-atmos.gsfc.nasa.gov>.

[13] Three data processing cycles were implemented since the beginning of MODIS data acquisition on 24 February 2000 (see Figure 4). The version 2 data were produced prior to November 2000 and version 3 from November 2000 to October 2002. The “consistent year” data set was designed to cover November 2000 to October 2001 without algorithm changes. The version 4 processing is planned from February 2000 through October 2003. The important changes made in version 4 for aerosol retrieval over land include: (1) the extension of aerosol retrievals over land from  $\rho_s^{2.1\mu\text{m}} < 0.15$  (in versions 2 and 3) to  $\rho_s^{2.1\mu\text{m}} < 0.25$  for both 0.47 and 0.66  $\mu\text{m}$  wavelengths and further to  $\rho_s^{2.1\mu\text{m}} < 0.4$  for 0.47  $\mu\text{m}$  only assuming continental aerosol model with reduced quality, (2) the

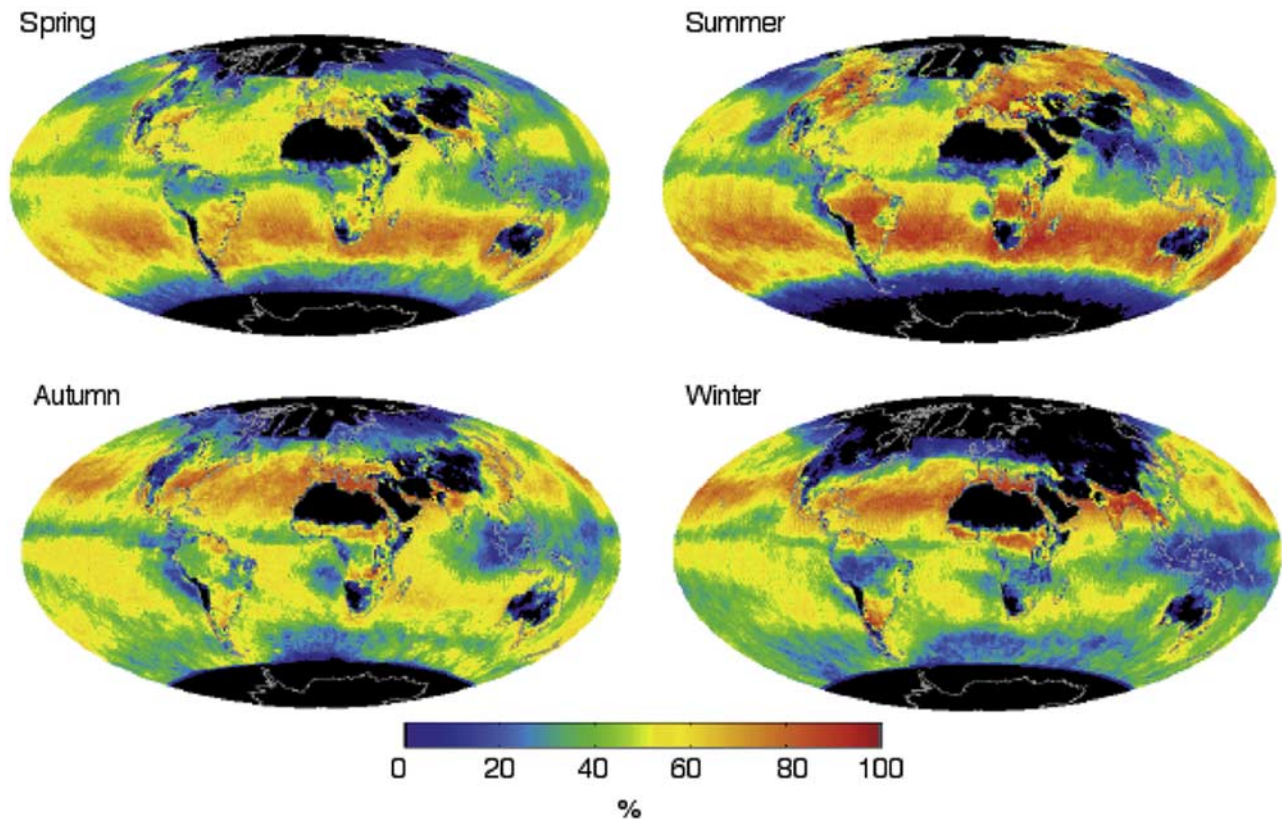


**Figure 6a.** Frequency maps of MODIS aerosol retrievals for spring (March–May 2001), summer (June–August 2001), autumn (September–November 2001), and winter (December 2000–January 2001). Frequency (%) is calculated using MODIS L3 daily products as the number of days with successful retrievals in  $1^\circ \times 1^\circ$  grids divided by the total number of calendar days in the season. Filled value (e.g., -9999) is filled in grids with unsuccessful retrieval. Note that a single retrieval from a  $10 \times 10$  km<sup>2</sup> area of L2 is allowed to represent a  $1^\circ \times 1^\circ$  area of L3.

substitution of 10–40 percentile by 20–50 percentile to reduce bias in selecting dark pixels but remain effective in minimizing contaminations as previously stated, (3) the addition of a heavy absorption smoke model ( $\omega_0 \sim 0.85$ – $0.86$ ) to account for biomass burning in southern Africa, and (4) the replacement of urban/industrial model ( $\omega_0 \sim 0.96$ ) with moderate absorption smoke model ( $\omega_0 \sim 0.96$ ) in eastern China and eastern Europe to better characterize aerosol absorption in those regions. The preliminary results of version 4 show a large increase in number of retrievals in southern Africa, eastern Europe, India, and eastern China but no change over deserts. In this paper, only versions 2 and 3 data are used.

#### 4. Results

[14] EOS-Terra MODIS sensor captured numerous aerosol events since launch. Figure 5 shows the highlights of snapshot aerosol events around the world. The  $\tau_a$  values at  $0.55 \mu\text{m}$  wavelength are interpolated between MODIS-derived  $\tau_a$  at  $0.47$  and  $0.66 \mu\text{m}$  in order to map together with ocean aerosol retrievals. Each image represents a L2 granule in the scale of  $2030 \text{ km}$  (length of 203 scans)  $\times$   $2330 \text{ km}$  (swath width). The black area over land shows no retrieval due to insufficient number of dark pixels ( $<10\%$  of a total of 400 pixels in a  $10 \times 10 \text{ km}^2$  grid box) because of

clouds, bright surfaces (e.g., deserts, snow/ice covered area), water bodies, or due to out-of-bound of lookup tables (e.g., Sun-satellite geometry). Over ocean, the black area represents no retrieval due to cloud cover, Sun glint, or out-of-bound of lookup tables.

[15] Figure 6a shows, by season and for each  $1^\circ \times 1^\circ$  grid, the percentage of days with successful retrievals from December 2000 to November 2001. Note that a single retrieval from a  $10 \times 10 \text{ km}^2$  of L2 is allowed to represent  $1^\circ \times 1^\circ$  area of L3. Frequency less than 100% is due to cloud cover (e.g., Southeast Asia and India affected by Asian summer monsoon), nonvegetated land surface (e.g., Sahara Desert, Taklimakan Desert, Gobi Desert, Tibetan Plateau, Antarctica, and Greenland), or missing data (due to instrument or data processing software related issues). At high latitude ( $>40^\circ\text{N}$  or  $40^\circ\text{S}$ ), more retrievals are seen because of the overlapping of satellite orbits. Figure 6b shows the corresponding images of seasonal mean  $\tau_a$  at  $0.55 \mu\text{m}$  (Northern Hemisphere). It is clear to see the springtime Asian dust outbreaks spreading over Northern Hemisphere, the shift of African dust outflow with latitude in different seasons, and the dry season biomass burning in southern Africa and South America. The dry season biomass burning in southern Africa and South America are the most pronounced aerosol events over land, followed by the springtime dust outbreaks in east Asia and summertime urban/

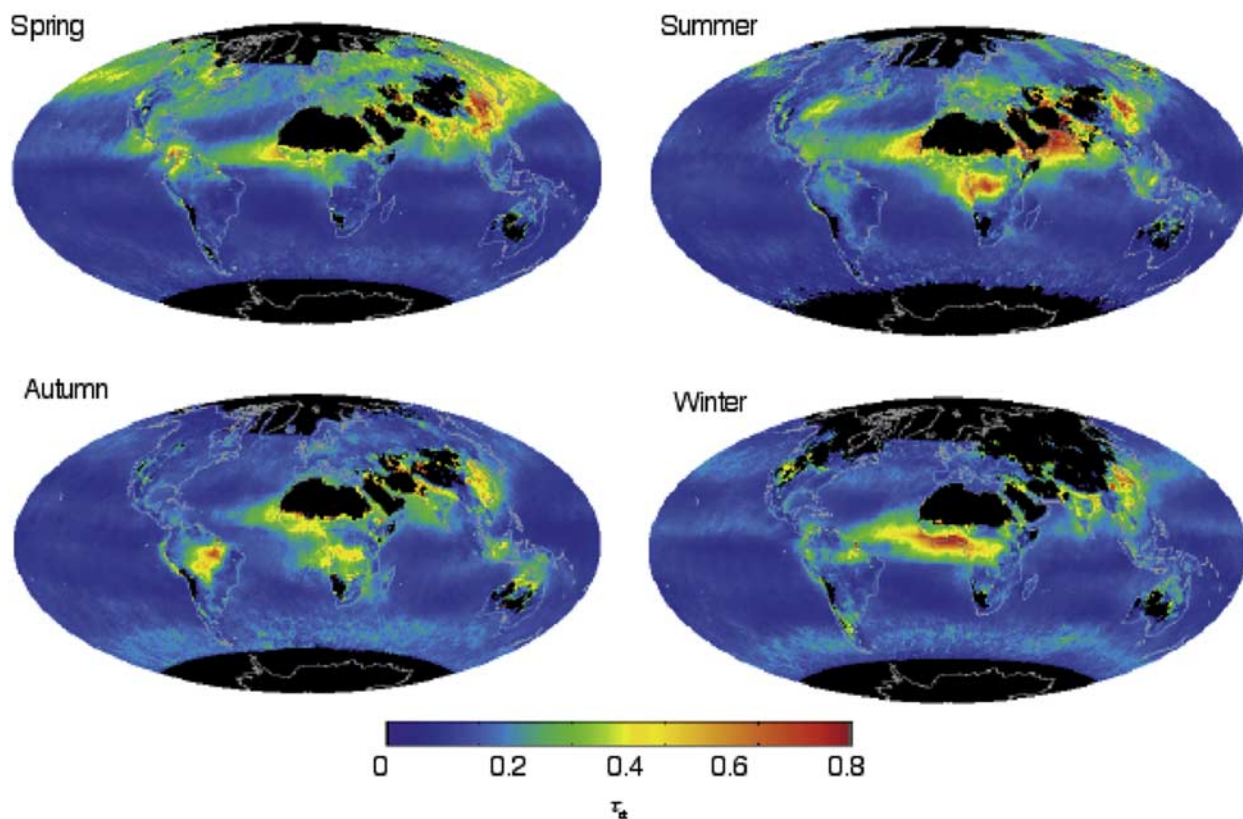


**Figure 6b.** Images of MODIS seasonal mean  $\tau_a$  for spring (March–May 2001), summer (June–August 2001), and autumn (September–November 2001), and winter (December 2000–February 2001). The seasonal mean  $\tau_a$  is calculated from MODIS L3 daily products.

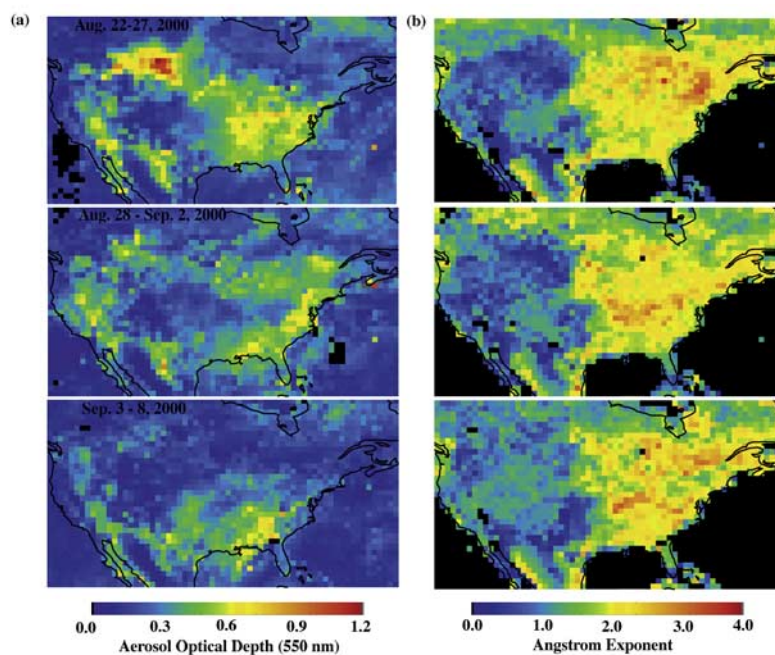


**Figure 7.** Images of 6-day average of MODIS L3 (a)  $\tau_a$  and (b)  $\alpha$  over the United States for 22–27 August 2000, 28 August to 2 September, and 3–8 September 2000.

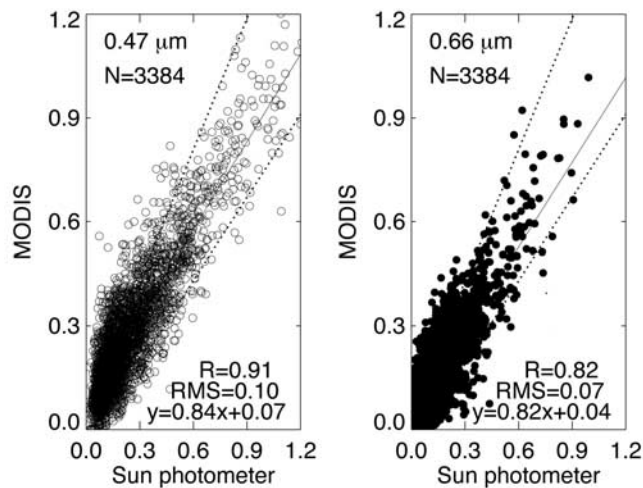


**Figure 8.** Global comparison of MODIS- and AERONET-derived  $\tau_a$  at 0.47 and 0.66  $\mu\text{m}$  wavelengths encompassing 3384 points from the eastern United States, western Europe, eastern Europe, east Asia, South America, and southern Africa. The solid lines represent the slopes of linear regression and the dotted lines the MODIS aerosol retrieval errors of  $\Delta\tau_a = \pm 0.05 \pm 0.20\tau_a$ .

industrial pollution in eastern China, India, the eastern United States, and western Europe.

[16] Ångström exponent ( $\alpha$ ), a quantity measuring the spectral dependence of  $\tau_a$ , is the most commonly used indicator of aerosol types, for example,  $\alpha > 1.5$  for the presence of man-made pollution or biomass burning aerosol and  $\alpha < 0.6$  for dust or sea salt (over ocean only). The MODIS-derived  $\alpha (= -\ln(\tau_a^{0.47\mu\text{m}}/\tau_a^{0.66\mu\text{m}})/\ln(0.47/0.66))$  reveal reasonable correlation with urban/industrial pollution (e.g., North America, Europe, China, and India) and biomass-burning (e.g., Brazil and southern Africa) aerosols [Chu *et al.*, 2002]. Figures 7a and 7b show the images of 6-day average of  $\tau_a$  and  $\alpha$  over the United States in three time periods: 22–27 August (heavy smoke plume from Montana/Idaho forest fires), 28 August to 2 September (lingering smoke), and 3–8 September 2000 (smoke free). Clearly, the smoke originated from western states forest fires enhanced the aerosol loading in the eastern United States (without much change in  $\alpha$ ) when transported to the east.

## 5. Validation

[17] More than 100 AERONET Sun photometers are operated daily to measure daytime aerosols [Holben *et al.*, 1998]. The wide distribution of AERONET stations, together with good calibration and data quality, better characterize global aerosol properties. Therefore we use AERONET measurements as the baseline validation for MODIS aerosol retrievals. However, there are regions (e.g., Asia) where AERONET measurements are scarce. Local Sun photometer measurements are adopted as an alternative validation source.

### 5.1. MODIS Versus AERONET Measurements

[18] In order to take into account both spatial and temporal variabilities, MODIS retrievals and AERONET direct

Sun measurements need to be colocated in space and time. The criteria adopted require at least 2 out of possible 5 AERONET measurements within  $\pm 30$  min of MODIS overpasses and at least 5 out of possible 25 MODIS retrievals within  $50 \times 50 \text{ km}^2$  centered at AERONET sites. The use of  $50 \times 50 \text{ km}^2$  (versus  $30 \times 30 \text{ km}^2$ ) box is primarily to obtain enough samples for statistical analysis. Given the average travel speed of aerosol mass on the order of 50 km/h, the  $50 \times 50 \text{ km}^2$  box size would match a 1-hour Sun photometer data segment [Ichoku *et al.*, 2003]. The differences resulted from  $50 \times 50 \text{ km}^2$  and  $30 \times 30 \text{ km}^2$  boxes may be larger close to biomass burning source regions ( $\sim 0.1$ – $0.2$ ) but they are not statistically significant according to the SAFARI 2000 results.

[19] The scatterplot in Figure 8 shows the global validation of MODIS-derived  $\tau_a$  against AERONET measurements from August 2000 to July 2002, which encompasses  $\sim 3400$  points from the eastern United States/Canada, western Europe, eastern Europe, east Asia, South America, and southern Africa. The slopes ( $S_l$ )  $\sim 0.82$ – $0.84$  and small intercepts ( $I_c$ )  $\sim 0.04$ – $0.07$  illustrate overall good agreement between MODIS and AERONET with correlation coefficients ( $R$ ) in the range of  $\sim 0.82$ – $0.91$ . The root-mean square (RMS) errors of  $\sim 0.07$ – $0.1$  reveal small biases due to aerosol model assumptions, surface reflectance estimate, and instrument calibration.

[20] The regional validation of summertime haze in the Northern Hemisphere (e.g., the eastern United States/Canada, western Europe) and dry season biomass burning in the Southern Hemisphere (e.g., southern Africa and South America) from July to September 2000 depicts that nearly all MODIS-derived  $\tau_a$  values fall within the range of retrieval error of  $\Delta\tau_a = \pm 0.05 \pm 0.20\tau_a$  with  $R$  in the range of  $\sim 0.92$ – $0.98$  at 0.47  $\mu\text{m}$  and  $\sim 0.85$ – $0.94$  at 0.66  $\mu\text{m}$  [Chu *et al.*, 2002]. Figures 9a and 9b show the comparisons between MODIS- and AERONET-derived  $\tau_a$  in the eastern United States/Canada and South America with dominant urban/industrial and biomass burning aerosol, respectively. The small  $I_c \sim 0.01$  in Figures 9a and 9b revealed the best estimate of surface reflectance as anticipated for vegetated surfaces (e.g., evergreen, deciduous, mixed forests, and cropland) in the eastern United States and Brazil since the relationship was derived based upon TM, AVIRIS, and MODIS Airborne Simulator measurements in Sulfate, Clouds, and Radiation-Atlantic (SCAR-A) and Smoke, Clouds, and Radiation-Brazil (SCAR-B) field experiments [Kaufman *et al.*, 1997a; Chu *et al.*, 1998]. Smaller deviation of slopes from unity is found at 0.47  $\mu\text{m}$  ( $\leq 0.06$ ) than at 0.66  $\mu\text{m}$  ( $> 0.1$ ). The value of  $S_l \sim 0.86$  at 0.66  $\mu\text{m}$  (see Figure 9b) disagrees with previous validation ( $S_l \sim 0.97$ ,  $I_c \sim 0.03$ ,  $R \sim 0.98$ ) assuming the single scattering albedo ( $\omega_o$ ) = 0.9 [Chu *et al.*, 1998], which is most likely due to the interannual variation of aerosol properties or the calibration drift (especially worse at 0.66  $\mu\text{m}$ ) of AERONET Sun photometer measurements. In the coastal zone of the eastern United States (e.g., NASA GSFC, Wallops Island, and Maryland Science Center) the overestimated MODIS  $\tau_a$  values ( $S_l \sim 1.16$ – $1.20$ ,  $I_c \sim 0.05$ – $0.09$ ,  $R \sim 0.90$ – $0.96$ ) are caused by surface inhomogeneity or subpixel water contamination [Chu *et al.*, 2002].

[21] MODIS aerosol retrievals in regions with occurrence of urban/industrial or biomass-burning aerosol are based on

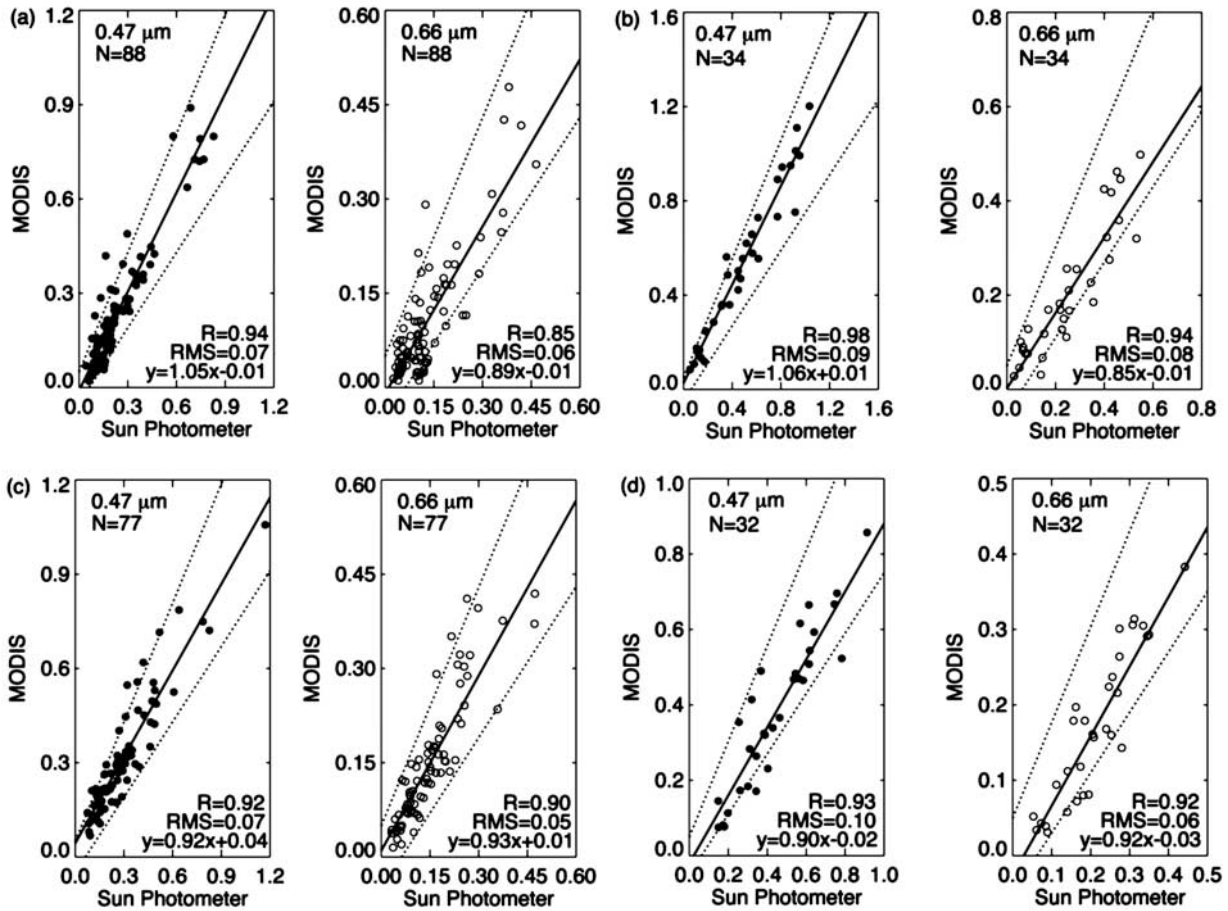


**Figure 9.** Comparisons of MODIS and AERONET derived  $\tau_a$  in (a) the eastern United States, (b) South America, (c) western Europe, and (d) southern Africa from July to September 2000. The solid lines represent the slopes of linear regression and the dotted lines the MODIS aerosol retrieval errors of  $\Delta\tau_a = \pm 0.05 \pm 0.20\tau_a$ .

the aerosol model derived from SCAR-A or SCAR-B as stated earlier. Table 2 shows the single scattering albedos of different aerosols derived by AERONET at different locations [Dubovik et al., 2002]. The similar values of  $S_I$  and  $I_c$  shown in Figure 9c (i.e., western Europe) versus those in Figure 9a (i.e., the eastern United States) imply that the differences, if any, in aerosol particle size and chemical composition are too small to affect the retrievals. The  $S_I$  values deviating from 1 ( $\sim 0.90$  at  $0.47 \mu\text{m}$  and  $\sim 0.92$  at  $0.66 \mu\text{m}$ ) in Figure 9d (southern Africa) are caused by higher black carbon content generated from biomass burning in southern Africa than South America. In other words, lowering  $\omega_o$  would produce a better fit, which is in agreement with  $\omega_o$  values derived by Dubovik et al. [2002] (smaller  $\omega_o$  values in southern Africa than South America). A new set of lookup tables ( $\omega_o \sim 0.85\text{--}0.86$ ) are added (in version 4) to account for the stronger absorption in southern Africa based upon the findings from SAFARI 2000 experiment [Eck et al., 2003].

**5.2. MODIS Versus Non-AERONET Measurements**

[22] AERONET measurements are scarce in Asia. Though several AERONET Sun photometers were deployed in China, Korea, and Japan during ACE-Asia

experiment, they are mainly focused on dust outbreaks from March to May 2001. Therefore local Sun photometer measurements serve as an alternative validation source for air pollution aerosol. Here we compare MODIS-derived  $\tau_a$  with handheld Sun photometers developed at Peking

**Table 2.** Single Scattering Albedos Derived From AERONET Measurements<sup>a</sup>

	$\omega_o, 0.44 \mu\text{m}$	$\omega_o, 0.66 \mu\text{m}$
<i>Urban/Industrial Aerosol</i>		
GSFC	0.98	0.97
Creteil/Paris	0.94	0.93
Mexico City	0.92	0.90
<i>Biomass Burning Aerosol</i>		
Amazonian Forest	0.94	0.93
South American Cerrado	0.91	0.89
African Savanna	0.89	0.85
<i>Dust Aerosol</i>		
Bahrain/Persian Gulf	0.93	0.95
Solar Village/Saudi Arabia	0.92	0.96
Cape Verde	0.93	0.98

<sup>a</sup>From Dubovik et al. [2002].

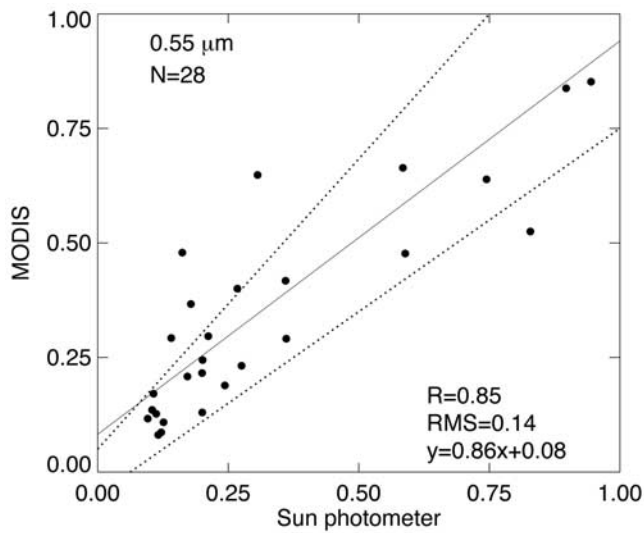


**Figure 10.** Comparisons of MODIS-derived  $\tau_a$  and SPU measurements from May to November 2001. SPU data are within  $\pm 1$  hour of MODIS overpass times and MODIS  $\tau_a$  values are obtained within 10 km in radius from SPU site. The solid lines represent the slopes of linear regression and the dotted lines the MODIS aerosol retrieval errors of  $\Delta\tau_a = \pm 0.05 \pm 0.20\tau_a$ .

University (hereinafter SPU), Beijing, China. The handheld SPU features 10 spectral channels from 0.44–0.91  $\mu\text{m}$ . Six channels (0.441, 0.497, 0.550, 0.607, 0.657, 0.863  $\mu\text{m}$ ) are used to measure aerosol and the rest (0.700, 0.764, 0.810, 0.910  $\mu\text{m}$ ) measure water vapor and oxygen absorption. SPU are frequently calibrated at Tibetan Plateau (elevation  $\sim 5$  km) with calibration accuracy  $\sim 1\%$  (J. Mao et al., personal communication, 2002). The SPU measurements used here were obtained between 10:00 and 13:00 local solar time (LST) from May to November 2001. Figure 10 shows the comparison between SPU measurements averaged within  $\pm 1$  hour of MODIS overpasses (10:45 a.m.  $\pm 40$  min) and MODIS-derived  $\tau_a$  obtained within 10 km in radius from SPU site. Except for a few outliers, most of the points fall within the retrieval errors. Beijing is geographically located at the boundary of two different ecosystems (semiarid and cropland) and Peking University (39.99°N, 116.31°E) is situated at the joint between urban area and mountains in the northwest of Beijing. As indicated by  $I_c \sim 0.14$ , surface inhomogeneity is responsible for the overestimation of aerosol loading derived by MODIS when  $\tau_a \leq 0.4$ . Aerosol composition (especially black carbon) is believed to play a significant role in underestimating aerosol loading when  $\tau_a > 0.4$ . Based upon the findings from local measurements of  $\omega_o \sim 0.85\text{--}0.90$  (J. Mao et al., personal communication, 2002), the replacement of urban/industrial model ( $\omega_o = 0.96$ ) with moderate absorption

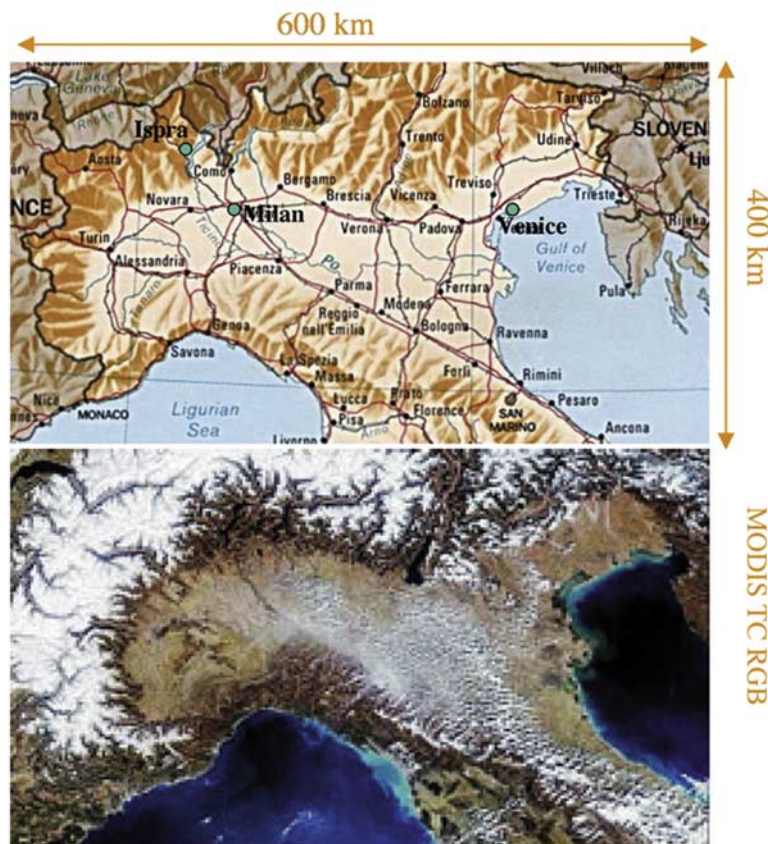


**Figure 11a.** (top) Geographic map and (bottom) topographic map of northern Italy (MODIS true color image) in the scale of  $600 \times 400 \text{ km}^2$ .

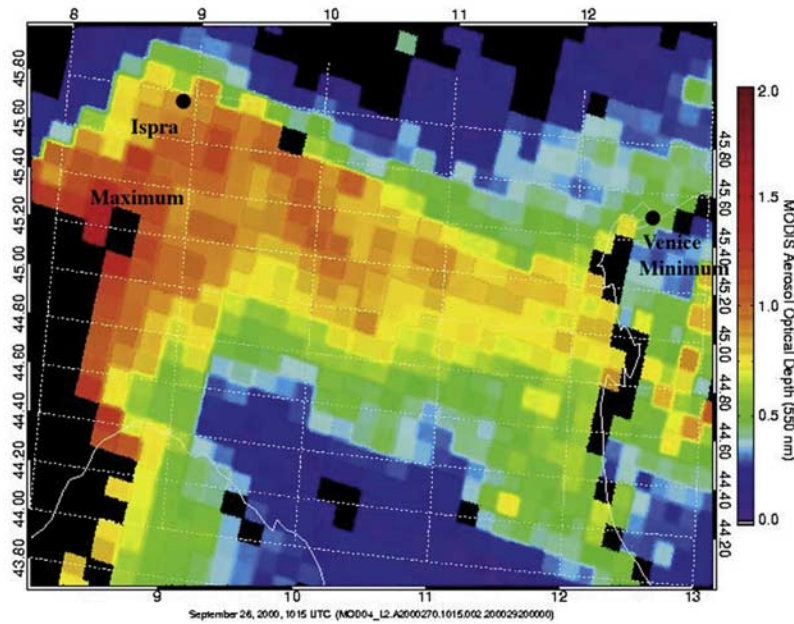


**Figure 11b.** Image of MODIS L2  $\tau_a$  at  $0.55 \mu\text{m}$  for the heavy pollution in northern Italy extending from the foot of Mt. Alps to Venice Lagoon on 26 September 2000 (10:15 UTC).

smoke model ( $\omega_o \sim 0.90$ ) would improve MODIS aerosol retrievals ( $\tau_a > 0.4$ ) in the region.

**6. Applications to Regional and Local Pollution: Case Studies**

[23] One important issue needed to address is whether MODIS aerosol retrievals (at  $10 \times 10 \text{ km}^2$  grid size) are applicable to regional or local air pollution. Presented here are three case studies: (1) northern Italy ( $\sim 600 \times 400 \text{ km}^2$ ), (2) city of Los Angeles ( $\sim 100 \times 50 \text{ km}^2$ ), and (3) Urban area of Beijing ( $\sim 30 \times 30 \text{ km}^2$ ). Note that these three cases only represent a small ensemble of aerosol events observed by MODIS. For most of the cases, the lack of ground truths make the verification and validation not possible. Figure 11a depicts the geographic and topographic maps of

northern Italy with the Alps transverse from west to northeast and the Apennines lying in the south. The Alps block the moisture of westerly from northern Atlantic Ocean. Therefore the climate in the south of the Alps is hot and dry in the summer and mild and wet in the winter. Figure 11b shows heavy air pollution observed by MODIS on 26 September 2000 (10:15 UTC) extending over 300 km from the west foothills of the Alps ( $\tau_a > 1.0$ ) to Venice Lagoon ( $\tau_a \sim 0.4$ ). In the heart of Po Valley, Milan, home to many international and local industrial plants, is considered to be the largest pollution source in the region. In the northwest of Milan at Ispra, the MODIS-derived  $\tau_a$  values ( $\sim 0.85$ ) reveal good agreement with AERONET Sun photometer observations ( $\sim 1.0$ ) at 10:15 UTC satellite overpass, which are more than double the September monthly mean  $\sim 0.43$  (or annual mean  $\sim 0.32$ ). Also shown a pick

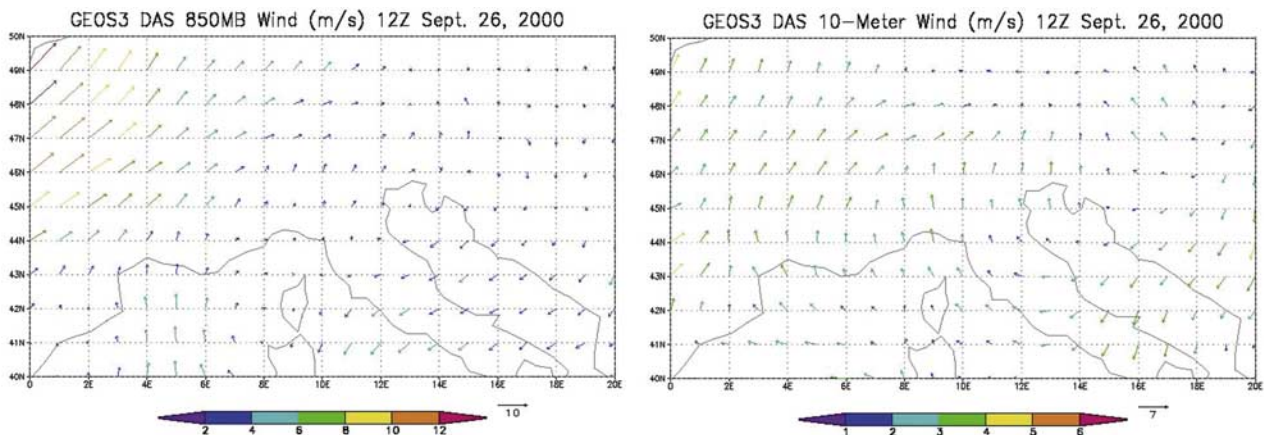


**Figure 11c.** GEOS-3 assimilated winds (left) at 850 hPa and (right) at 10 m above surface in the region of  $40^\circ\text{--}50^\circ\text{N}$  and  $0^\circ\text{--}20^\circ\text{E}$ .

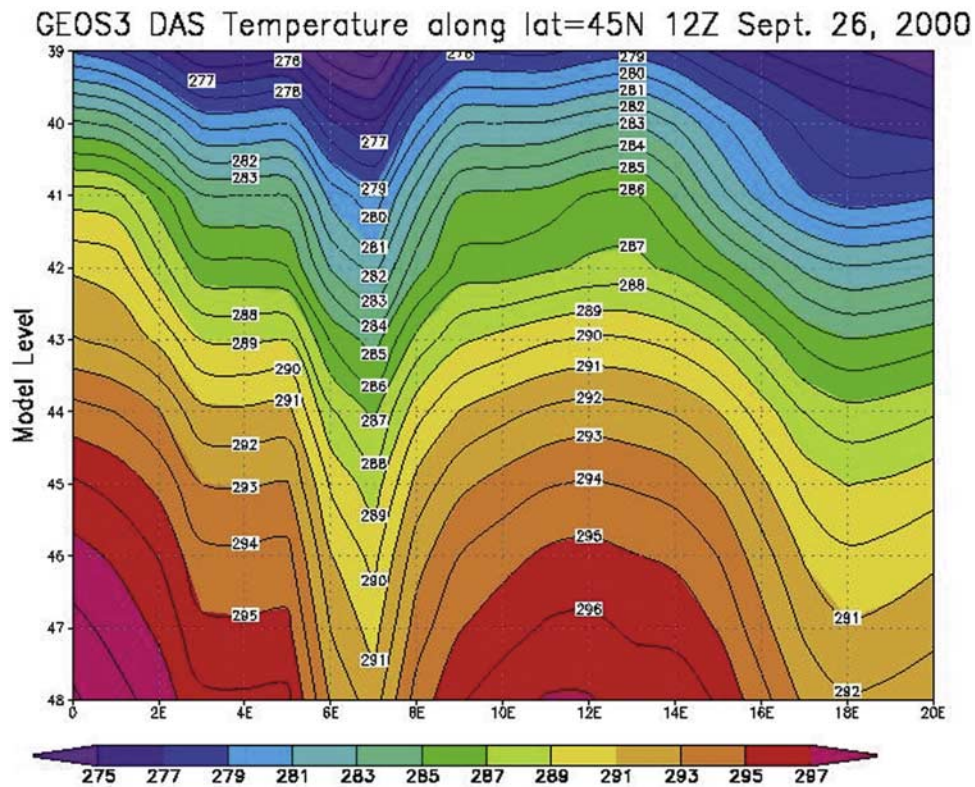


**Figure 11d.** GEOS-3 assimilated temperature profile along 45°N between 0° and 20°E in northern Italy. The model level 48 to 39 denotes surface to 700 hPa.

value of  $\sim 52 \mu\text{g}/\text{m}^3$  on 26 September the daily  $\text{PM}_{10}$  (particle size  $< 10 \mu\text{m}$  in diameter) mass concentration measured at surface is a result of steady increase of pollutants from  $6 \mu\text{g}/\text{m}^3$  (cf. MODIS-derived  $\tau_a \sim 0.1$ ) on 22 September after severe rain events. Under stagnant condition, stable air masses allow pollutants to continuously accumulate before being removed by wind or precipitation. In the downwind region near Venice Lagoon, the MODIS-derived  $\tau_a$  ( $\sim 0.45$ ) and AERONET Sun photometer measurements ( $\sim 0.4$ ) are found to be more comparable with the September monthly mean  $\sim 0.34$  (or annual mean  $\sim 0.30$ ), indicating less variability in the downwind as opposed to the source region. Though the location of Venice site ( $\sim 8$  nautical miles off Venice Lagoon) is considered maritime, the aerosol type is typically continental because most aerosols are transported from the nearby valley.

[24] To analyze meteorological conditions associated with the air pollution event, we use NASA DAO GEOS-3 data with improved dynamics and physics [Takacs et al., 1999; Conaty et al., 2000]. The assimilated data output every 6 hours (model time step  $\sim 100$  seconds s) including 48 vertical layers (surface: 0.01 hPa) at  $1^\circ \times 1^\circ$  resolution. On 26 September (12:00 UTC) the wind field at 850 hPa shows a weak clockwise circulation centered near Gulf of Venice (left panel of Figure 11c). Light onshore flows ( $\sim 1\text{--}2$  m/s) are seen at the south of the Alps, for instance, along  $44^\circ\text{N}$  latitude between  $12^\circ\text{--}14^\circ\text{E}$ . Stronger southeast winds ( $\sim 2\text{--}3$  m/s) are shown at 10-m altitude (right panel of Figure 11c) for a 3-hour average from 9:00 to 12:00 UTC. The assimilated wind speeds are generally in good agreement with surface measurements ( $\sim 1\text{--}2$  m/s) over the entire region.

No temperature inversion was found above the heavy aerosol layer (see Figure 7d). In the stagnant Mediterranean summer, air pollution particles in northern Italy are corralled between the Alps and the Apennines. The agreement of MODIS and AERONET-derived  $\tau_a$  at Ispra (error  $\leq 0.15$ ) and Venice (error  $\leq 0.05$ ), and the second-order polynomial fit of aerosol retrievals between Ispra and Venice (see

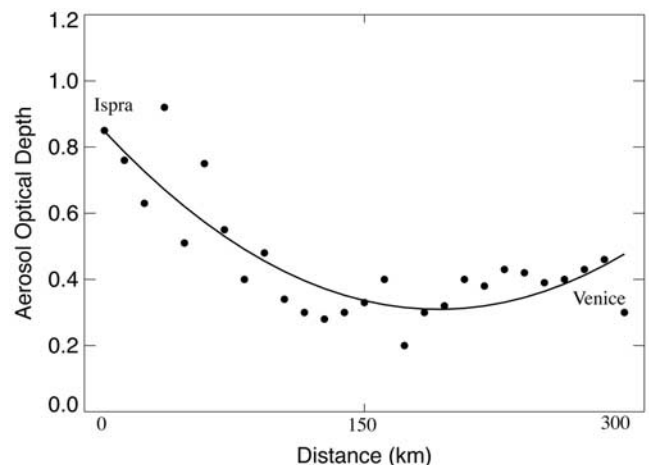


**Figure 11e.** MODIS L2  $\tau_a$  values (black dots) derived between Ispra ( $\sim 1.0$ ) and Venice ( $\sim 0.4$ ) as shown by the transection (straight line) in Figure 11b. Gray dot represents AERONET Sun photometer measurements and solid line the second polynomial fit of MODIS-derived  $\tau_a$  values.

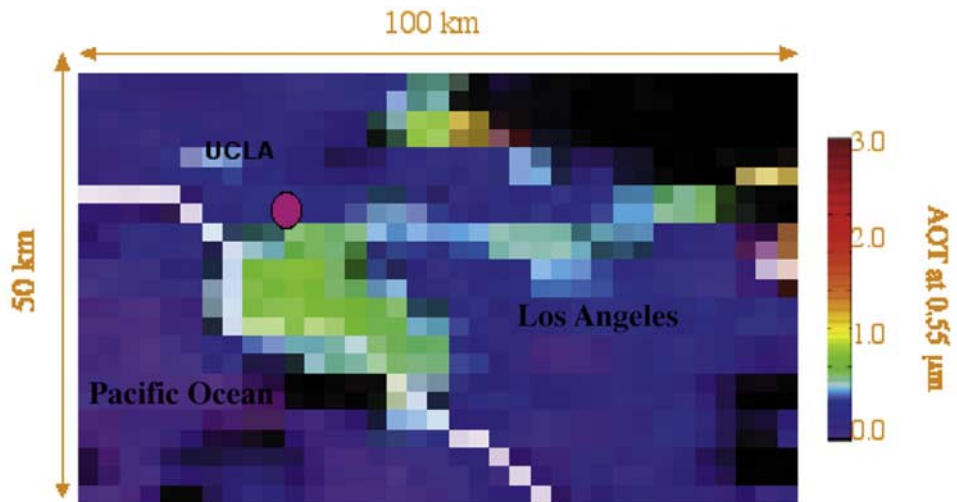
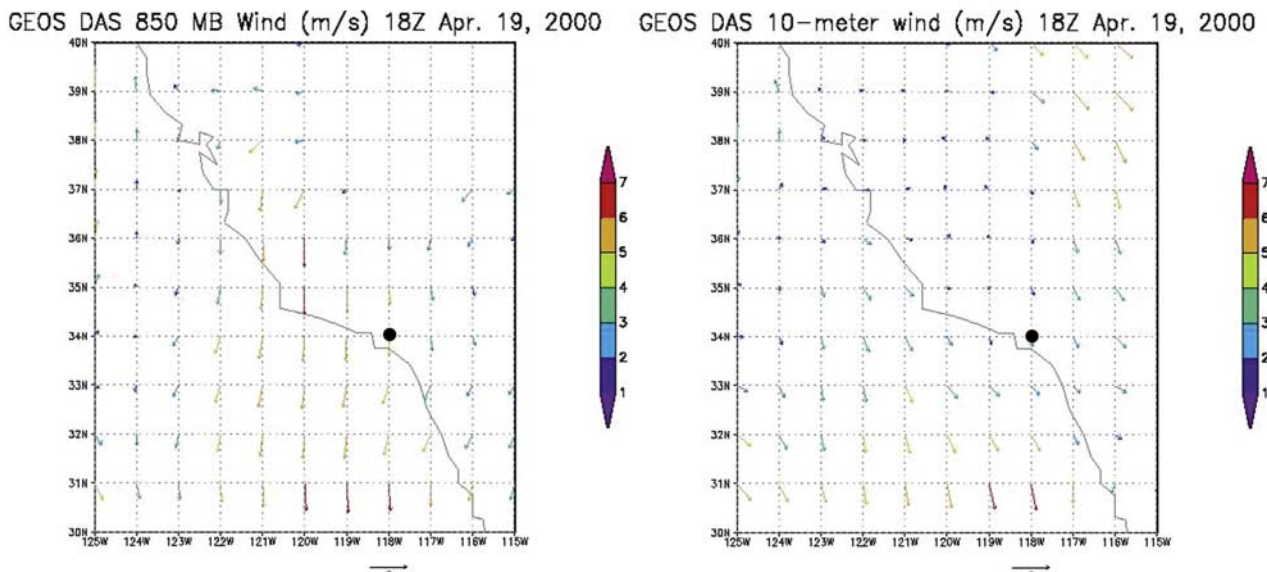


Figure 12a. Image of MODIS L2  $\tau_a$  at 0.55  $\mu\text{m}$  in the vicinity of Los Angeles on 19 April 2000.



Figure 12b. (top) Locations of urban/industrial regions and highways (yellow-marked area). (bottom) TM image of topography around Los Angeles (terrain and hills are shown as dark in the image).



**Figure 12c.** GEOS-3 assimilated winds (left) at 850 hPa and (right) at 10 m above surface in the region of 30°–40°N and 115°–125°W. Black dot denotes the location of AERONET UCLA site (34°N, 118°W).

Figure 11e) depict not only the accuracy but also the spatial sensitivity of MODIS aerosol retrievals.

[25] A question immediately rising is whether MODIS aerosol retrievals at  $10 \times 10 \text{ km}^2$  are good enough to resolve smaller-scale air pollution. The measurements acquired on 19 April 2000 (18:35 UTC or 10:35 a.m. LST) over Los Angeles provided us a chance to answer this question. From Figure 12a, it is clear to see that

MODIS-derived  $\tau_a$  coincide with urban/industrial areas and highways (i.e., yellow-marked area in Figure 12b). As enhanced by a high-pressure system  $\sim 300\text{--}400 \text{ km}$  offshore in the west and a low-pressure system in the east of Los Angeles, stronger northerly winds of  $\sim 5\text{--}6 \text{ m/s}$  were observed at 850 hPa (see Figure 12c) compared to the northwesterly of 2–3 m/s at 10m altitude. Without temperature inversion, the combination of light wind (2–3 m/s)

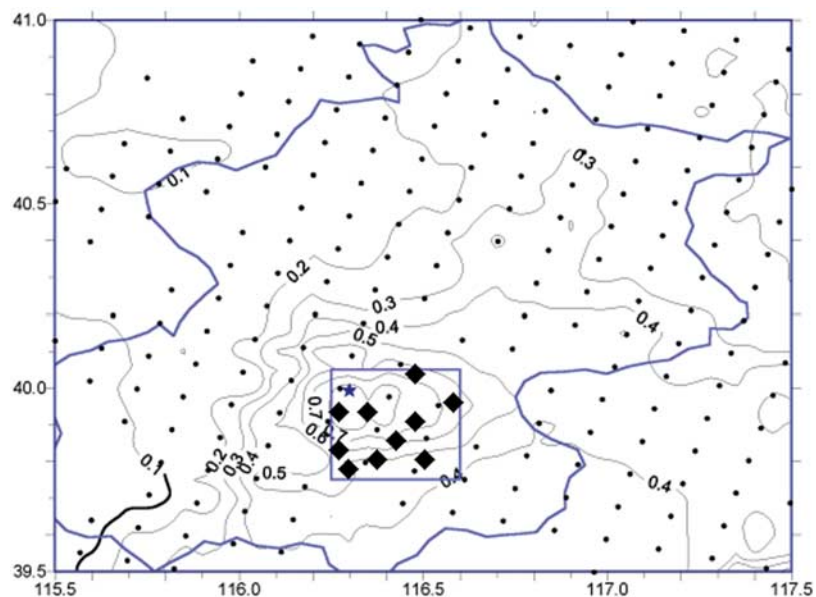


**Figure 13.** Contour plot of MODIS-derived  $\tau_a$  around SPU site (blue star) on 17 May 2001 (3:00 UTC). Irregular outline represents the boundary of city of Beijing and the rectangle box represents the Beijing urban area. X axis denotes the longitude (°E) and y axis the latitude (°N). Diamond indicates the location of  $\text{PM}_{10}$  sites.

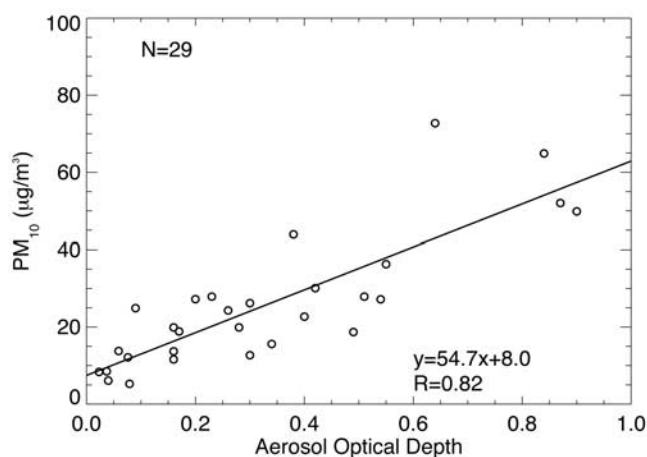


**Figure 14.** Relationship between 24-hour  $PM_{10}$  concentrations and daily averaged AERONET  $\tau_a$  measurements from August to October 2000 in northern Italy.

with slight onshore component and surrounding terrain prevented pollutants from being removed. The 24-hour mass concentrations observed about 20 miles from UCLA (University of California at Los Angeles,  $118.45^\circ W$ ,  $34.07^\circ$ ) depict  $PM_{10}$  values in the range of  $15\text{--}20\ \mu g/m^3$ . In the vicinity the spatially collocated but not temporally matched MODIS aerosol retrievals show  $\tau_a$  values  $\sim 0.3\text{--}0.4$ . The agreement between aerosol optical depths derived from MODIS ( $\tau_a \sim 0.33$ ) and AERONET ( $\tau_a \sim 0.3$ ) at UCLA (collocated in space and time) indicates the potential of using MODIS  $\tau_a$  retrievals in monitoring city pollution. Shown next is the case study in Beijing, China with much higher aerosol loading and  $PM_{10}$  concentration.

[26] With growing population and the increase in the number of automobiles, the air quality in Beijing becomes an increasing concern to the local government. In spring, dust outbreaks from western China and Mongolia frequently passed through the capital city, adding to already worsened air quality due to emission from automobiles and nearby

power plants and factories. The case selected here is purposely to avoid the influence of dust storm because of larger errors in MODIS retrievals using  $2.1\ \mu m$ . Figure 13 shows the contour plot of MODIS aerosol retrievals (black dots) on 17 May 2001 (3:00 UTC, or 11:00 LST); SPU site is denoted as black star at the northwest of urban area of Beijing. One can see that the surrounding mountains (elevation  $\sim 2\ km$ ) caused the sharp gradient of  $\Delta\tau_a \sim 0.7$  in a distance of  $20\text{--}30\ km$  at the west and north of Beijing. Around the SPU site, the MODIS-derived  $\tau_a \sim 0.84$  is shown in good agreement with observed  $\tau_a \sim 0.89$  by SPU. Corresponding to the aerosol optical depth is a  $PM_{10}$  concentration of  $\sim 330\ \mu g/m^3$  (averaged over 10 urban stations in 24 hours), which is  $\sim 50\%$  larger than the monthly mean ( $\sim 226\ \mu g/m^3$ ) and approximately  $\sim 2$  times the annual mean ( $\sim 170\ \mu g/m^3$ ). On 16 May, the  $PM_{10}$  concentration of  $\sim 500\ \mu g/m^3$  was recorded in correspondence to the MODIS-derived  $\tau_a \sim 0.64$  (or SPU  $\tau_a \sim 0.75$ ). Based upon local meteorological data, the presence of temperature inversion layer at  $\sim 700\ m$  in the morning hours is considered to be a major contributing factor to the large  $PM_{10}$  values. However, the mismatch of the  $PM_{10}$  concentrations and MODIS columnar aerosol loading (i.e.,  $330\ \mu g/m^3$  and  $\tau_a \sim 0.84$ ,  $500\ \mu g/m^3$  and  $\tau_a \sim 0.64$ ) suggests other factors also need to take into account. The rapid change in wind speed and direction (typically in spring) caused by the afternoon mountain-valley effect, capable of generating blowing dusts from construction sites (e.g., buildings and roads) could have contributed to the extreme  $PM_{10}$  concentration.

[27] The factors that can hinder the relationship between MODIS-derived columnar  $\tau_a$  and  $PM_{10}$  concentration measured at surface include aerosol vertical distribution, type, properties, and temporal variability. The MODIS validation with AERONET [Kaufman *et al.*, 1997a; Chu *et al.*, 1998, 2002; Ichoku *et al.*, 2003] or Ames Airborne Tracking Sun Photometer (AATS) [Schmid *et al.*, 2003] shows that most errors found in aerosol retrievals are attributed to the underestimation of single scattering albedo (e.g., biomass burning in southern Africa and pollution in eastern China)

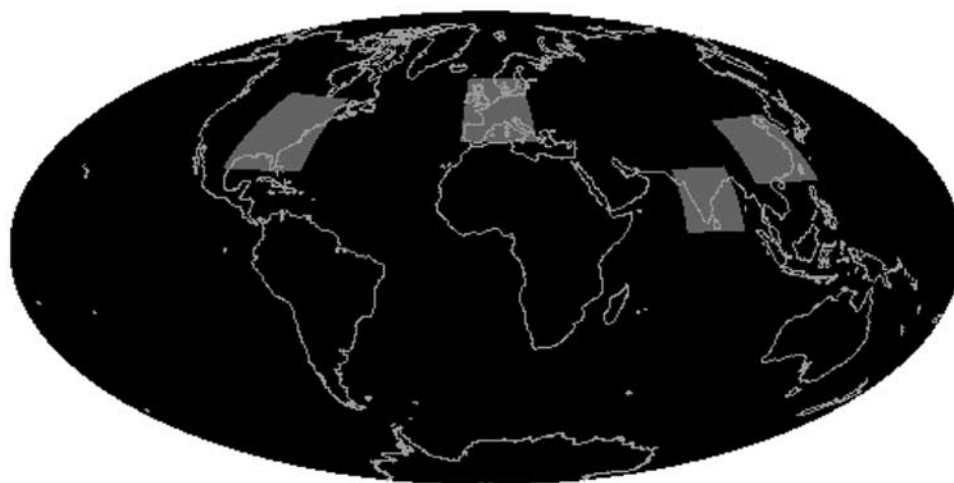


**Figure 15.** Four selected regions: eastern China ( $20\text{--}40^\circ N$ ,  $100\text{--}125^\circ E$ ), India ( $5\text{--}25^\circ N$ ,  $70\text{--}90^\circ E$ ), the eastern United States and Canada ( $25\text{--}50^\circ N$ ,  $70\text{--}100^\circ W$ ), and western Europe ( $37\text{--}60^\circ N$ ,  $10^\circ W\text{--}20^\circ E$ ) for the analysis of monthly mean  $\tau_a$  (over land only).

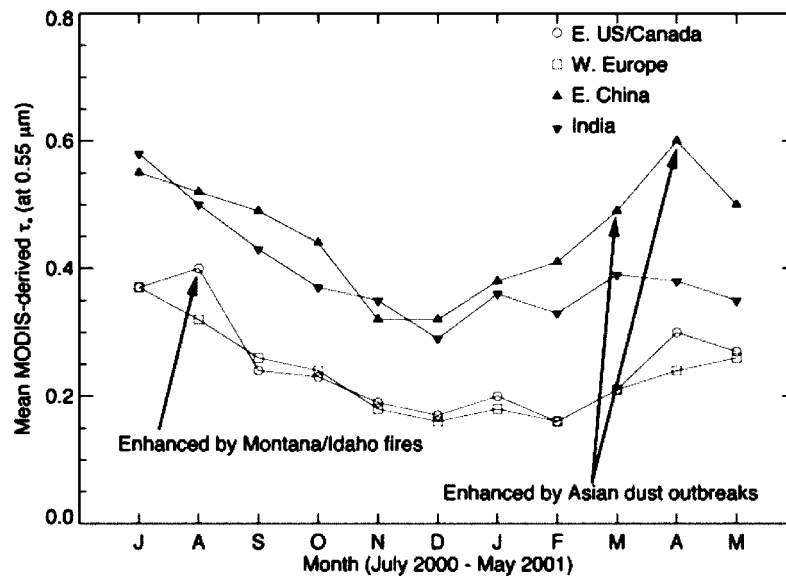


**Figure 16.** Time series of monthly mean  $\tau_a$  for eastern China, India, the eastern United States/Canada, and western Europe between July 2000 and May 2001.

or surface reflectance estimate (e.g., coastal zones). Since  $\tau_a$  represent the integrated aerosol loading of atmospheric columns, the relationship of  $\tau_a$  and  $\text{PM}_{10}$  is naturally dependent upon aerosol vertical distribution. In addition, because of the differences in aerosol chemical composition affecting particle extinction (scattering and absorption) efficiency and hygroscopicity, aerosol type and properties can also alter the linear regression, not to mention the temporal variability of aerosols. Given a high correlation coefficient (e.g.,  $>0.8$ ), the slope derived from linear regression can be seen as the “conversion factor” between columnar aerosol optical depth and  $\text{PM}$  mass concentration, and the intercept is the error of the conversion.

[28] In the absence of hourly  $\text{PM}$  measurements in northern Italy, we match 24-hour  $\text{PM}_{10}$  concentration with daily averaged AERONET  $\tau_a$  at Ispra from August to October 2000. The stable air masses and fixed pollution sources are believed to produce such good correlation of  $R \sim 0.82$  with a slope  $\sim 55 \mu\text{g}/\text{m}^3$  and very small intercept  $\sim 8 \mu\text{g}/\text{m}^3$  (see Figure 14). This case is unique to show the good correlation obtained between the daily averaged  $\tau_a$  and  $\text{PM}_{10}$  concentration because the topography in northern Italy allows pollutants to accumulate under stagnant condition without mixing with other types of aerosol. In contrast, the case in Beijing is much more complicated. The lack of hourly  $\text{PM}$  and aerosol vertical profile measurements prohibits us to obtain any reasonable regression between columnar  $\tau_a$  and  $\text{PM}_{10}$  mass concentration.

## 7. Regional and Temporal Variability of Aerosol Optical Depth

[29] The analysis of aerosol optical depth (at  $0.75 \mu\text{m}$ ) observed from 46 stations in China clearly showed an upward trend of annual mean increased from 0.35 to 0.45 between 1960 and 1990 [Luo *et al.*, 2001]. Since 1990, the economic development in China has moved at an even faster pace and thus the increase in aerosol loading is

expected to be greater. The launch of EOS-Terra MODIS in December 1999 was just in time to monitor the fast developing world. Here we compare the monthly mean  $\tau_a$  of four regions: two most populated regions (eastern China and India) and two most industrialized regions (the eastern United States/Canada and western Europe) (see Figure 15). Note that only MODIS-derived  $\tau_a$  over land are used. It is clear that the monthly means of eastern China and India are at least 50% to 2–3 times larger than those in the eastern United States/Canada and western Europe from July 2000 to May 2001 (see Figure 16), which is in line with the projected sulfur dioxide emission from Asia ( $\sim 60$  million tons) as opposed to that from the United States/Canada and Europe combined ( $\sim 30$  million tons) in 2000 [Downing *et al.*, 1997]. The time series of monthly mean  $\tau_a$  also depicts a strong seasonal variation with maxima in the spring/summer and minima in the winter, and with enhancements from smoke in August 2000 as originated from the Montana/Idaho forest fires transported to the eastern United States and dust outbreaks from Taklimakan and Gobi Deserts to east Asia as well as smoke from Southeast Asia to south China during springtime (February–April) 2001. The large standard deviations ( $\sim 50$ – $60\%$  of monthly means) derived from the calculations reflect the high spatial variability of MODIS aerosol retrievals in the source regions.

## 8. Concluding Remarks

[30] MODIS aerosol retrievals provide useful perspective to the global air pollution. The three case studies in northern Italy, Los Angeles, and Beijing demonstrated the MODIS capability for monitoring regional and local air pollution. With Terra and Aqua MODIS direct broadcasting (data processing time  $<1$  hour), the near real time (twice a day) monitoring of air pollution is possible in any places around the world. The regression ( $R \sim 0.82$ ,  $S_I \sim 55 \mu\text{g}/\text{m}^3$ ,  $I_c \sim 8 \mu\text{g}/\text{m}^3$ ) obtained between AERONET-derived  $\tau_a$  and

PM<sub>10</sub> concentration in northern Italy (as a result of stable air masses and fixed pollution sources) showed the potential of using MODIS aerosol product as a decision tool in air quality applications (e.g., assessment and forecast). In less idealized conditions, such as in Beijing, China, there are factors (e.g., aerosol vertical profile, aerosol type and properties, temporal variability, etc.) needed to take into account. As such, there is currently no useful information on a global scale between columnar aerosol optical depth and mass concentration measured at surface. The spaceborne lidar measurements from Geoscience Laser Altimeter System (GLAS) launched in January 2003 and Cloud-Aerosol Lidar and Infrared Pathfinder Satellite Observations (CALIPSO) scheduled to launch in 2004 may be sufficient, if not 100%, to characterize aerosol vertical distribution, which should help us understand and improve the relationship between aerosol optical depth and PM mass concentration worldwide.

[31] The identified sources of retrieval error, such as subpixel clouds, snow/ice, and water contamination are important for the improvements of MODIS aerosol retrievals. Equally important are the characterization of uncertainties of aerosol and land surface properties in places beyond the scope of field experiments (SCAR-A, SCAR-B, SAFARI 2000, ACE-Asia). Transcontinental aerosols when mixed with local pollution not only change the vertical distribution but also modify the chemical composition, which can pose significant difficulties in accurately retrieving aerosol properties. Nevertheless, MODIS's ability to derive aerosol optical depth over land has made significant progress in quantifying columnar aerosol amount in the source region. Today's measurements in the eastern United States and western Europe comparing to eastern China and India suggest the results of reduced air pollution level because of continuous governmental clean-air activities.

[32] **Acknowledgments.** The authors would like to thank MODIS science data support team for processing level 2 and level 3 data, and AEROENT PIs for collecting aerosol observations around the world. Special thanks go out to Jean-Philippe Putaud of Joint Research Center for providing the particulate matter data of Ispra EMEP station and Mark Gray of MODIS atmosphere team for providing imaging processing software.

## References

- Ackerman, S. A., et al., Discriminating clear-sky from clouds with MODIS, *J. Geophys. Res.*, *103*, 32,141–32,158, 1998.
- Adriano, D. C., and A. H. Johnson, *Acidic Precipitation*, vol. 2, *Biological and Ecological Effects*, Springer-Verlag, New York, 1989.
- Beeson, W. L., D. E. Abbey, and S. F. Knutsen, Long-term concentrations of ambient air pollutants and incident lung cancer in California Adults: Results from the AHSMOG Study, *Environ. Health Perspect.*, *106*, 813–822, 1998.
- Braslau, N., and J. V. Dave, Effect of aerosols on the transfer of solar energy through realistic mode atmosphere, part I: Non-absorbing aerosols, *J. Appl. Meteorol.*, *12*, 601–615, 1973.
- Chameides, W. L., et al., Case study of the effects of atmospheric aerosols and regional haze on agriculture: An opportunity to enhance crop yields in China through emission control, *Proc. Natl. Acad. Sci. USA*, *96*, 13,626–13,633, 1999.
- Charlson, R. J., S. E. Schwartz, J. M. Hales, R. D. Cess, J. A. Coakley Jr., J. E. Hansen, and P. J. Hoffman, Climate forcing of anthropogenic aerosols, *Science*, *255*, 423–430, 1992.
- Christopher, S. A., D. A. Kliche, J. Chou, and R. M. Welch, First estimate of the radiative forcing of aerosols generated from biomass burning using satellite data, *J. Geophys. Res.*, *101*, 21,265–21,273, 1996.
- Chu, D. A., et al., Remote sensing of smoke from MODIS airborne simulator during SCAR-B experiment, *J. Geophys. Res.*, *103*, 31,979–31,987, 1998.
- Chu, D. A., Y. J. Kaufman, C. Ichoku, L. A. Remer, D. Tanré, and B. N. Holben, Validation of MODIS aerosol optical depth retrieval over land, *Geophys. Res. Lett.*, *29*(12), 8007, doi:10.1029/2001GL013205, 2002.
- Conaty, A. L., et al., The structure and evolution of extratropical cyclones, fronts, jet streams, and the tropopause in GEOS general circulation model, *Bull. Am. Meteorol. Soc.*, *82*, 1853–1867, 2000.
- Dave, J. V., and J. Gazdag, A modified Fourier transform method for multiple scattering calculation in a plane parallel Mie atmosphere, *Appl. Opt.*, *9*, 1457–1466, 1970.
- Diner, D. J., et al., Multi-angle Imaging Spectroradiometer (MISR) description and experiment overview, *IEEE Trans. Geosci. Remote Sens.*, *36*, 1072–1087, 1998.
- Downing, R., R. Ramankutty, and J. Shah, Global environmental trends, RAINS-ASIA: An assessment model for acid deposition in Asia, World Resour. Inst., Washington, D. C., 1997. (Available at <http://www.wri.org/wri/>.)
- Dubovik, O., et al., Variability of absorption and optical properties of key aerosol types observed in worldwide locations, *J. Atmos. Sci.*, *59*, 590–608, 2002.
- Eck, T. F., et al., Variability of biomass burning aerosol optical characteristics in southern Africa during the SAFARI 2000 dry season campaign and a comparison of single scattering albedo estimates from radiometric measurements, *J. Geophys. Res.*, *108*(D13), 8477, doi:10.1029/2002JD002321, 2003.
- Gatebe, C. K., et al., Sensitivity of off-nadir zenith angle to correlation between visible and near-infrared reflectance for use in remote sensing of aerosol over land, *IEEE Trans. Geosci. Remote Sens.*, *39*(4), 805–819, 2001.
- Hansen, J. E., and A. A. Lacis, Sun and dust versus greenhouse gases: An assessment of their relative roles in global climate change, *Nature*, *346*, 713–719, 1990.
- Herman, J. R., P. K. Bhartia, O. Torres, N. C. Hsu, C. J. Sefort, and E. Celarier, Global distribution of UV-absorbing aerosols from Nimbus-7/TOMS data, *J. Geophys. Res.*, *102*, 16,911–16,922, 1997.
- Holben, B. N., et al., AERONET—A federated instrument network and data archive for aerosol characterization, *Remote Sens. Environ.*, *66*, 1–16, 1998.
- Hsu, N. C., et al., Detection of biomass burning smoke from TOMS measurements, *Geophys. Res. Lett.*, *23*, 745–748, 1996.
- Hsu, N. C., J. R. Herman, and C. Weaver, Determination of radiative forcing of Saharan dust using combined TOMS and ERBE data, *J. Geophys. Res.*, *105*, 20,649–20,661, 2000.
- Ichoku, C., L. A. Remer, Y. J. Kaufman, R. Levy, D. A. Chu, D. Tanré, and B. N. Holben, MODIS observation of aerosols and estimation of aerosol radiative forcing over southern Africa during SAFARI 2000, *J. Geophys. Res.*, *108*(D13), 8499, doi:10.1029/2002JD002366, 2003.
- Intergovernmental Panel on Climate Change (IPCC), *A Plan for a Research Program on Aerosol Radiative Forcing and Climate Change*, Natl. Acad. Press, Washington, D. C., 2001.
- Karnieli, A., Y. J. Kaufman, L. A. Remer, and A. Wald, AFRI—Aerosol free vegetation index, *Remote Sens. Environ.*, *77*, 10–21, 2001.
- Kaufman, Y. J., D. Tanre, L. A. Remer, E. F. Vermote, D. A. Chu, and B. N. Holben, Operational remote sensing of tropospheric aerosol over the land from EOS-MODIS, *J. Geophys. Res.*, *102*, 17,051–17,061, 1997a.
- Kaufman, Y. J., A. Wald, L. A. Remer, B.-C. Gao, R.-R. Li, and L. Flynn, The MODIS 2.1  $\mu\text{m}$  channel—Correlation with visible reflectance for use in remote sensing of aerosol, *IEEE Trans. Geosci. Remote Sens.*, *35*(5), 1286–1298, 1997b.
- Kaufman, Y. J., N. Gobron, B. Pinty, J.-L. Widlowski, and M. M. Verstraete, Relationship between surface reflectance in the visible and mid-IR used in MODIS aerosol algorithm - theory, *Geophys. Res. Lett.*, *29*(23), 2116, doi:10.1029/2001GL014492, 2002.
- King, M. D., Y. J. Kaufman, D. Tanré, and T. Nakajima, Remote sensing of tropospheric aerosols from space: Past, present and future, *Bull. Meteorol. Soc.*, *80*, 2229–2259, 1999.
- Luo, Y., D. Lu, X. Zhou, and W. Li, Characteristics of the spatial distribution and yearly variation of aerosol optical depth over China in last 30 years, *J. Geophys. Res.*, *106*, 14,501–14,513, 2001.
- Penner, J. E., R. J. Charlson, J. M. Hales, N. Laulainen, R. Leifer, T. Novakov, J. Ogren, L. F. Radke, S. E. Schwartz, and L. Travis, Quantifying and minimizing uncertainty of climate forcing by anthropogenic aerosols, *Bull. Am. Meteorol. Soc.*, *75*, 375–400, 1994.
- Remer, L. A., et al., Tropical biomass burning smoke aerosol size distribution model, *J. Geophys. Res.*, *103*, 31,879–31,892, 1998.
- Remer, L. A., et al., Validation of MODIS aerosol retrieval over ocean, *Geophys. Res. Lett.*, *29*(12), 8008, doi:10.1029/2001GL013204, 2002.

- Schmid, B., et al., Coordinated airborne, spaceborne, and ground-based measurements of massive thick aerosol layers during the dry season in southern Africa, *J. Geophys. Res.*, 108(D13), 8496, doi:10.1029/2002JD002297, 2003.
- Takacs, L. L., A. Mold, and S. Nebuda, On the impact of improved dynamics and physics in the GEOS-2 GCM, paper presented at 13th Conference on Numerical Weather Prediction, Am. Meteorol. Soc., Denver, Colo., 13–17 Sept. 1999.
- Tanré, D., Y. J. Kaufman, M. Herman, and S. Mattoo, Remote sensing of aerosol properties over oceans using the MODIS/EOS spectral radiances, *J. Geophys. Res.*, 102, 16,971–16,988, 1997.
- Tanré, D., et al., Retrieval of aerosol optical depth thickness and size distribution over ocean from MODIS airborne simulator during TARFOX, *J. Geophys. Res.*, 104, 2261–2278, 1999.
- Tegen, I., A. A. Lacis, and I. Fung, The influence on climate forcing of mineral aerosols from disturbed soils, *Nature*, 380, 419–422, 1996.
- Torres, O., P. K. Bhartia, J. R. Herman, Z. Ahmad, and J. Gleason, Derivation of aerosol properties from satellite measurements of backscattered ultraviolet radiation, Theoretical basis, *J. Geophys. Res.*, 103, 17,099–17,110, 1998.
- 
- J. D. Chern, GEST/Laboratory for Atmospheres, NASA/GSFC, Greenbelt, MD 20771, USA. (jchern@dao.gsfc.nasa.gov)
- D. A. Chu, Science Systems and Applications, Inc., 10210 Greenbelt Road, Suite 600, Lanham, MD 20706, USA. (achu@climate.gsfc.nasa.gov)
- B. N. Holben, Laboratory for Terrestrial Physics, Code 923, NASA/GSFC, Greenbelt, MD 20771, USA. (holben@aeronet.gsfc.nasa.gov)
- Y. J. Kaufman, Laboratory for Atmospheres, Code 913, NASA/GSFC, Greenbelt, MD 20771, USA. (kaufman@climate.gsfc.nasa.gov)
- C. Li and J. Mao, Department of Atmospheric Science, School of Physics, Peking University, Beijing 100871, China. (ccli@ust.hk; mjt@pku.edu.cn)
- G. Zibordi, Institute for Environment and Sustainability, Joint Research Centre, Ispra, Italy. (giuseppe.zibordi@jrc.it)